

Molecular Engineering on Kinetics-Driven Self-Assembled Monolayers Working as Auxiliary Layers on Dielectrics in Organic Field-Effect Transistors

Mingliang Li, Yingnan Cao, Kefeng Xie,* and Jinyao Tang*

Self-assembled monolayers (SAMs) are a class of quasi-2D materials adhesive to the substrate by chemisorption. Due to their transparency, diversity, stability, sensitivity, selectivity, and great potential in surface passivation, SAMs have been extensively investigated and applied in various functional devices, particularly in organic field effect transistors (OFETs). Among all the processing methods, kinetic-driven spin-coating is frequently used for the SAM preparation due to its high efficiency and low cost. However, the importance of SAM quality and its relationship to device performance has not been studied in detail, hindering the new SAM development and device optimization. In this study, SAMs prepared by kinetic-driven spin-coating are carefully investigated in terms of their surface morphology, density, and regularity, and proposed a correlation model between chemical structure and SAM quality. Additionally, the prepared SAMs are utilized as auxiliary layers on dielectrics and analyzed their effects on OFET properties. Through these investigations, a sequential relationship is established between chemical structure, SAM quality, and device performance, which can provide efficient feedback for system optimization.

selectivity and passivation ability, making them a promising tool for surface modification for modulating the wettability or improving the adhesion between different layers, even directly tuning the electronic structure of the adjacent layers.^[4–7] SAMs have been widely investigated and applied in various functional devices, including organic field effect transistors (OFETs)^[3,8,9], organic solar cells,^[10–11] and perovskite solar cells^[12–13] due to their structural diversity, low cost, and processing simplicity.^[5,14] Along with the most common solution incubation approach, spin-coating is also frequently used for the SAM preparation. In solution incubation, SAMs reach a thermodynamically-favorable near-equilibrium state with sufficient immersion time.^[15–16] Conversely, spin-coating, exhibiting a kinetic-driven feature during the rapid solvent volatilization, is more frequently adopted

for its high efficiency.^[13,17,18] However, reported works based on spin-coating processes usually ignore the SAM quality difference originating from their chemical structures and processing methods, particularly in SAM density and regularity. Limited evidence on SAM quality may not be sufficient to support the device functions, which impedes the development of effective SAM devices. For kinetic-driven spin-coating, a correlation between chemical structure, SAM quality, and device performance is urgently needed to complete the feed loop for the optimization of the device performance. To solve these problems, molecular engineering was performed by four SAM molecules with variant head groups in this work. The obtained SAMs by spin-coating were carefully investigated in terms of morphology, density, and packing regularity. A relationship model between chemical structure and SAM quality was established and further verified by theoretical calculation. Finally, OFETs with these SAMs as auxiliary layers on dielectrics were fabricated to investigate the influence of SAM microstructures on device performance, leading to a systematic relationship between chemical structure, SAM quality, and device performance.


As illustrated in **Figure 1**, a standard four-step spin-coating method was employed in this work. The four SAM molecules (PaC4, PaPh, PaCz, and PaBTBT) were prepared as a solution in advance and dropped onto oxygen plasma activated HfO₂

1. Introduction

Self-assembled monolayers (SAMs) are a class of amphiphilic compounds that can be chemisorbed onto the substrate resulting in a quasi-2D film.^[1–3] The unique structure of SAMs offers superior transparency, diversity, and stability, with high surface

M. Li, Y. Cao, J. Tang
Department of Chemistry
The University of Hong Kong
Hong Kong 999077, China
E-mail: jinyao@hku.hk

K. Xie
School of Chemistry and Chemical Engineering
Lanzhou Jiaotong University
Lanzhou 730070, China
E-mail: xiekefeng@mail.lzjtu.cn

 The ORCID identification number(s) for the author(s) of this article can be found under <https://doi.org/10.1002/aelm.202300712>

© 2023 The Authors. Advanced Electronic Materials published by Wiley-VCH GmbH. This is an open access article under the terms of the Creative Commons Attribution License, which permits use, distribution and reproduction in any medium, provided the original work is properly cited.

DOI: 10.1002/aelm.202300712

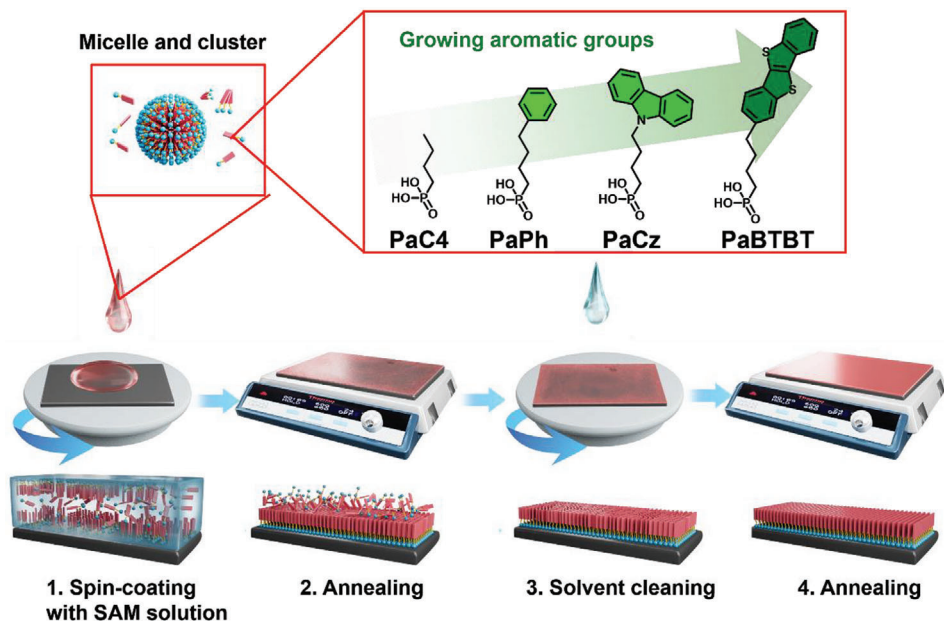


Figure 1. A schematic of the chemical structures of SAMs and the standard four-step spin-coating process.

substrates. Subsequently, the substrate was rotated on a stage to facilitate SAM formation during solvent volatilization. Hot-stage annealing can enhance surface passivation by promoting chemical bonding between the phosphonic-acid anchor and metal-oxide substrate. However, SAMs exhibit an amphiphilic nature, which often results in the formation of micelles or clusters in solution, thus multilayers during spin-coating.^[19–20] Therefore, an additional spin-coating with clean solvent is necessary to eliminate excess physisorbed molecules. Then SAMs are subjected to further annealing to remove the solvent residual and optimize the molecular packing, after that they are ready for characterization and device application.

2. Results and Discussion

The quality of the SAMs is investigated in terms of surface roughness, molecular density, and packing regularity. The surface microstructures are investigated by atomic force microscope (AFM) and scanning electron microscope (SEM). From the AFM images (**Figure 2a**; Figure S1, Supporting Information), the surface textures keep almost identical with slightly increased roughness after SAM modification (Figure 2b).^[22] SEM results also reveal similar morphology, and the characteristic elements in SAMs, including P, S, or N, were uniformly distributed on the substrate by energy dispersive spectroscopy (EDS) modules (Figure 2c; Figures S2 and S3, Supporting Information), indicating the absence of severe aggregations formed with the standard processing procedure.

X-ray photoelectron spectroscopy (XPS) was applied, benefiting from its high sensitivity. For example, with the signals of P and S in PaBTBT (Figure 2d; Figure S4, Supporting Information), the adhesion of SAMs on the HfO₂ substrates could be proven.^[21,23] Moreover, the element signal presents a shift when it is in different chemical environments.^[24–25] The O signals could be deconvoluted into three subpeaks by fitting, assigned to

Hf–O–Hf, Hf–OH, and Hf–O–P/P=O (Figure 2e).^[26] The subpeaks demonstrate the formation of SAM-surface bonding and provide detailed information on the chemical natures and contents of these bonds. As demonstrated in Figure 2f, the subpeak Hf–O–P/P=O originating from the SAM anchor group signified a decline in SAM density with the increase in head groups' size (Table S1, Supporting Information). Furthermore, the exact SAM coverages were revealed by UV–vis-spectroscopy-based method (UV–vis, Figure 2f; Table S3, Supporting Information).^[27] The densities of PaC4, PaPh, PaCz, and PaBTBT are calculated as 8.7, 6.6, 4.3, and 3.0 × 10^{−10} mol cm^{−2} and deliver areas per molecule (*S*) of 19.09, 25.17, 35.34, and 42.59 Å², respectively, which are consistent with the values estimated by density functional theory (DFT) and reported values for alkanethiolate SAMs (≈20 Å²).^[28,29]

The XPS measurements can also provide the content information for both the SAMs and the substrate within the detection depth of ≈5 nm.^[11] Therefore, a semi-quantitative analysis on the elemental contents by XPS was conducted to identify the regularity of SAMs (Figure 2g; Table S2, Supporting Information). As order packed molecule layer can shield the photoelectron from the bottom layer and attenuate the XPS signal, the difference coefficient between the atomic-sensitivity-factors-weighted C/P element ratio and the stoichiometric one (R_{ASF}/R_{number}), defined in Equation S1 (Supporting Information), is selected as an indicator of the molecular regularity in SAMs. Therefore, the R_{ASF}/R_{number} decreases with the molecular density, with the exception of PaBTBT, which exhibits the highest regularity with the lowest molecular density. The time-dependent contact angle measurements (Figure 2h; Table S4, Supporting Information) also support the observed SAM regularity order, as higher regularity of SAMs could slow down the permeation of water to the hydrophilic anchor and substrate, leading to better stability and longer decay time.^[17,30] Moreover, in the attenuated total reflection-Fourier transform infrared spectroscopy (ATR-FTIR) as shown in Figure S6 (Supporting Information), the shifts of two

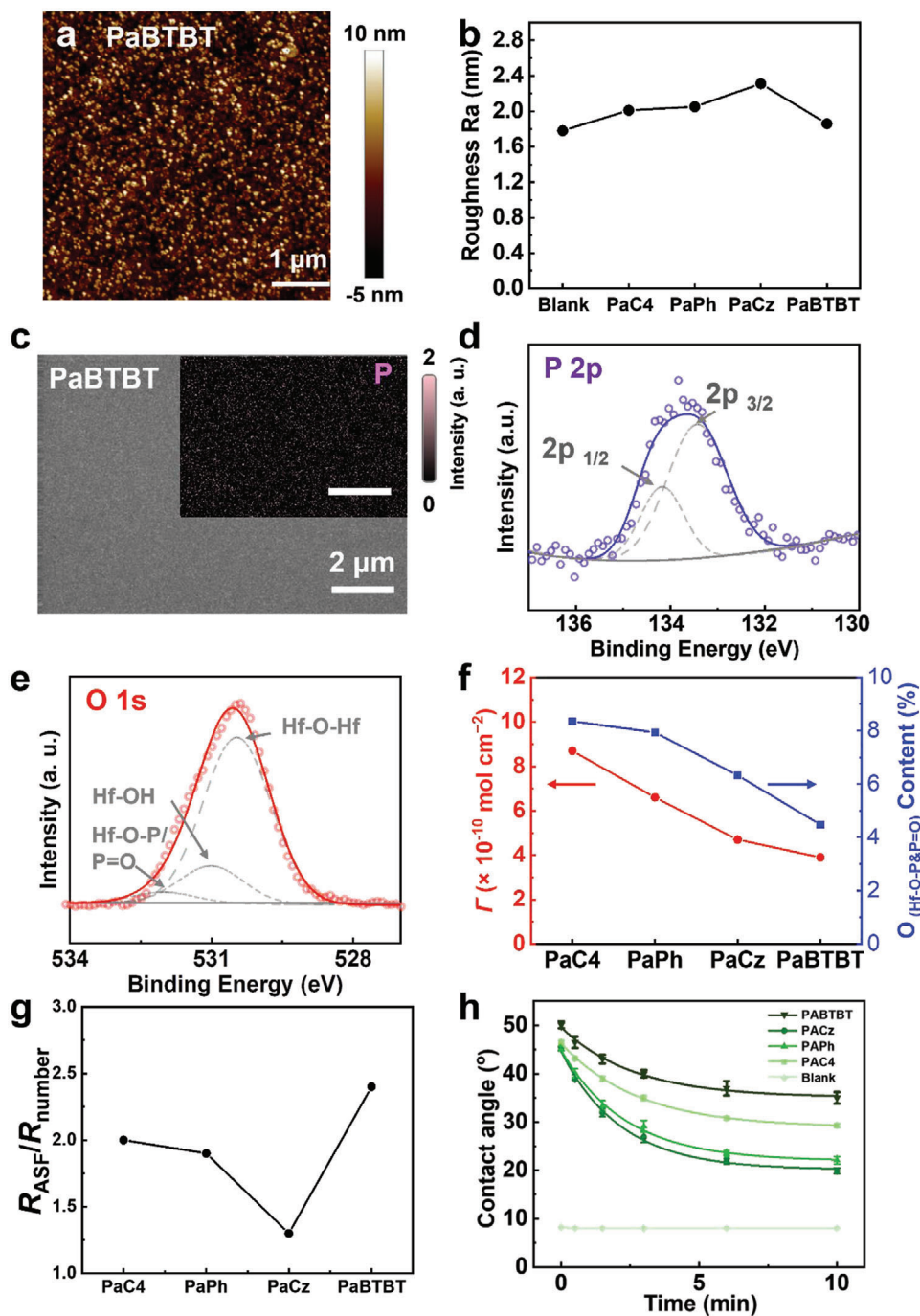


Figure 2. SAM quality characterizations. a) AFM image of PaBTBT SAM on HfO₂-coated substrate. b) Roughnesses of the SAMs from AFM images in Figure 2a and Figure S1 (Supporting Information). c) SEM image and P element EDS mapping (inset) of PaBTBT SAM. d, e) are high-resolution XPS element mappings of P 2p and O 1s, respectively. The P 2p peak at 133.3 eV consists of the two components: 132.8 eV (P 2p_{3/2}) and 133.6 eV (P 2p_{1/2}).^[21] f) Densities calculated from UV-vis spectra (red) and O (Hf-O-P/P=O) content in all O species (blue). g) Trends of R_{ASF}/R_{number} with the growing aromatic groups of SAMs. h) Trends of the parameters in time-dependent contact-angle tests of SAMs.

vibrations of C–H stretch (a symmetric stretch at ≈ 2851 cm⁻¹ and an asymmetric stretch at ≈ 2920 cm⁻¹) to the higher field evidence a disordered monolayer with cis C–C bonds,^[31,32] which indicate PaC4 and PaBTBT with the top regularity in alkyl linkers.

This difference in density and regularity should originate from molecular structure and interaction of the SAM head groups. With the expansion of the conjugation head group, the molecule's rigidity and size increase, which leads to a decrease in the density of the SAM during spin-coating due to the steric

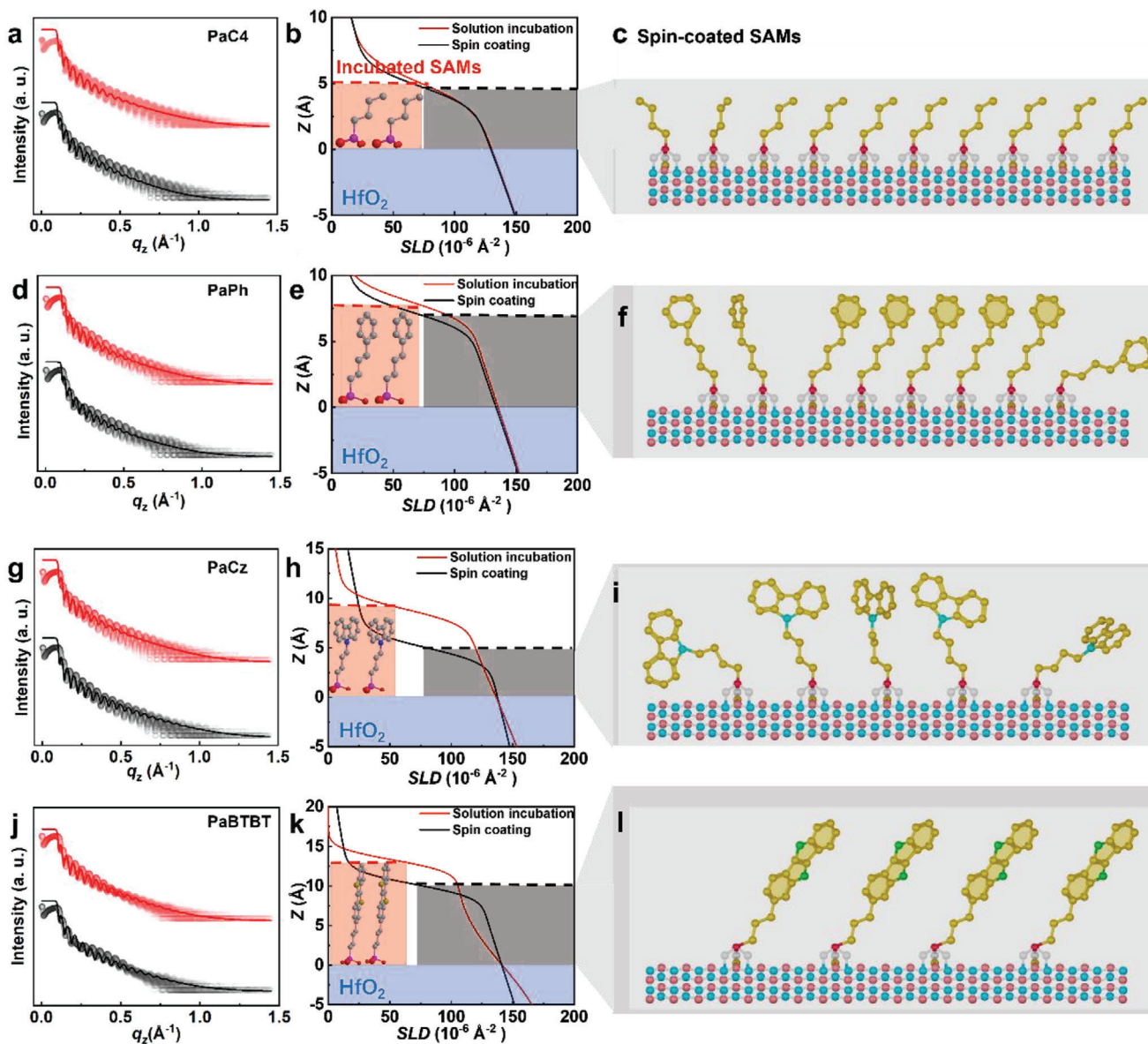


Figure 3. XRR measurements and the corresponding modeling on SAMs. a,d,g,i) are the XRR measurements of SAMs (dots) and the corresponding fitting curve (solid curves). b,e,h,k) are the scattering length density (SLD) profiles. Samples prepared by solution incubation and spin-coating are indicated as red and gray, respectively. c,i,f,l) are modeling of spin-coated SAMs.

effect. The small PaC4 and PaPh with good flexibility exhibit high density, allowing sufficient intermolecular interactions for high regularity. On the other hand, PaBTBT, with a big conjugated head group, could show strong π - π interaction even at a relatively low density to achieve exceptional regularity.

On this basis, X-ray reflectivity (XRR) measurements were performed to reveal the SAM thickness (Figure 3; Tables S5 and S6, Supporting Information).^[33] For comparison, the SAMs prepared by solution incubation were tested as ideally-packed film with near-equilibrium assembly. Evidenced by the fitting results, the SAM thickness of PaC4 and PaPh prepared using both methods show limited differences, while the spin-coated PaCz and PaBTBT are only 56.2% and 76.7% the thickness of the solution-

incubated SAMs, respectively, implying insufficient SAM packing.

By integrating the findings on SAM density and regularity, a structural model was developed to explain the formation of SAMs through kinetic-driven spin-coating. As the conjugated head group expands, the SAM density gradually decreases, resulting in a reduced SAM thickness and molecular regularity. However, when the π - π interaction outweighs the impact of SAM density (as is the case for BTBT in our study), film regularity may be restored with tilted molecular conformation.

In order to verify the molecular regularity in SAMs, theoretical calculations on molecular dynamics (MD) were carried out and presented in Figure S8 (Supporting Information). Vector ν was

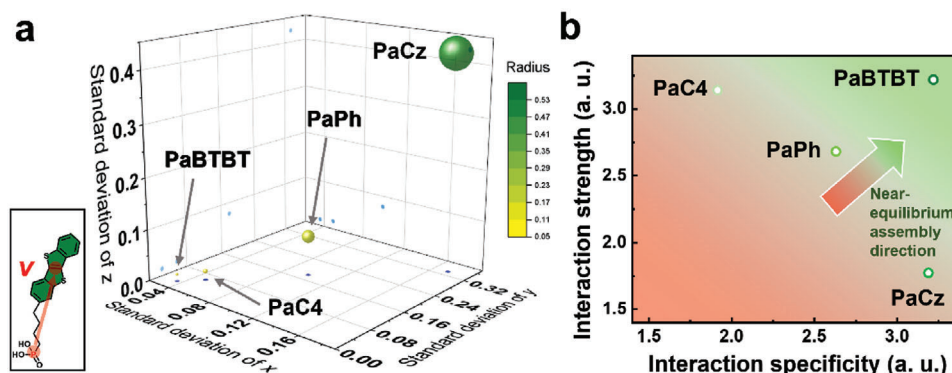


Figure 4. Theoretical calculations. a) Statistical standard deviation of SAM vector ν in MD calculations. The radius is the root mean square of standard deviations of the ν coordinates. The inset shows the definition of the SAM vector ν , which is from the P atom to the geometric center of the head group. b) Schematic phase diagram, as dictated by the direction of thermodynamic stability. Interaction strength and specificity were demonstrated by the binding energies of two identical and different SAM molecules from Table S7 (Supporting Information), respectively.

defined as the arrow from the phosphorus atom to the geometric center of the head molecule, and the 3D coordinates of the vector were statistically analyzed (Figure 4a). The degree of dispersion of the vector orientation was described by the root mean square of the coordinate standard deviation (demonstrated as the radius of the sphere in Figure 4a), and the results were found to be consistent with the regularity trend proposed in the model.

Molecular interactions are evaluated by the strength and specificity, which can be quantified by the binding energies between identical and different molecules from DFT calculation, respectively (Figure 4b; Table S7, Supporting Information). It was found

that PaBTBT can maintain both interaction strength and specificity superior to the other molecules, which makes it easy to reach the thermodynamically steady state during spin-coating.^[15]

To further investigate the correlation between SAM quality and device performance, an OFET device study was conducted with thermally-evaporated pentacene as a conductive-semiconductor layer and designed SAMs as the passivation surface layer on HfO_2 dielectrics (Figure 5a). As shown in Table S8 (Supporting Information), the capacitance value of SAMs decreases as the regularity grows. The devices were evaluated based on three key parameters: on/off ratio, mobility (μ), and threshold voltage (V_{th}),

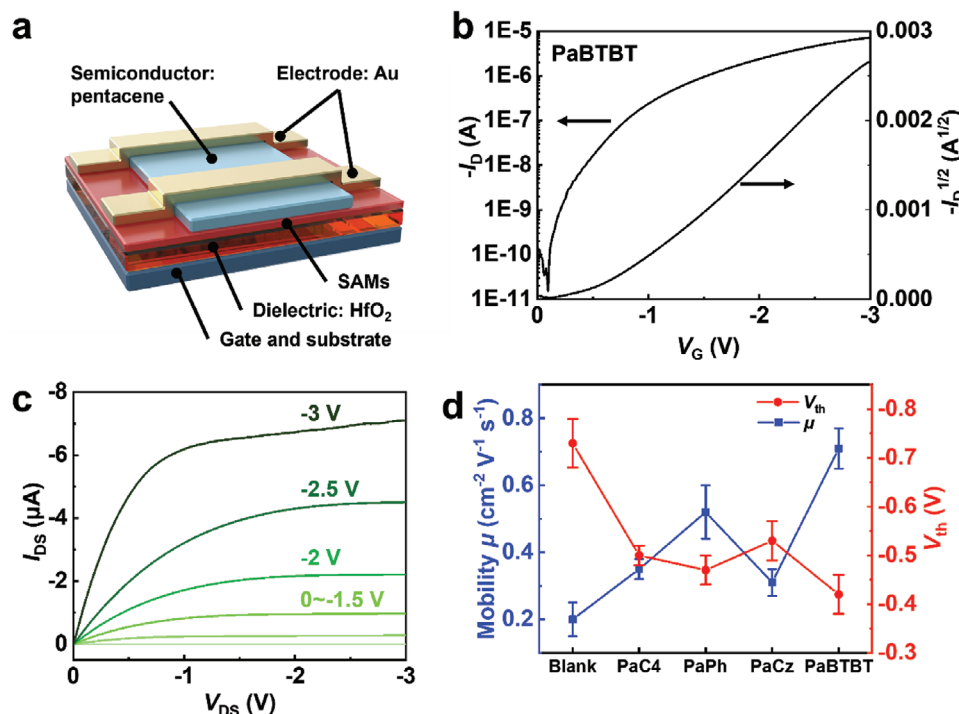


Figure 5. OFET device characterizations. a) Schematic cross-section of an OFET with SAMs working as general dielectric surface. b,c) are the transfer and output curves with PaBTBT SAM. The average on/off ratio is $\approx 10^5$. $L = 100 \mu\text{m}$ and $W = 1000 \mu\text{m}$. d) Mobilities and threshold voltages for SAM-decorated OFET devices.

using 30 devices for each type of SAM. The transfer and output curves of the devices are presented in Figure 5b,c, and Figure S10 (Supporting Information).

Evidenced by Figure 5d and Figure S11 (Supporting Information), the quality of SAMs has a significant impact on all three parameters. The developments of the μ and on/off ratio are basically consistent with the regularity of SAMs, which is attributed to the fact regularly-formed SAMs on the oxide dielectric can decrease the gate leakage current^[34] and improve the molecular packing at the adjacent semiconductor interface.^[35,36] Therefore, the device based on PaBTBT SAM with high regularity exhibits champion performance with an average μ of $0.71 \text{ cm}^{-2} \text{ V}^{-1} \text{ S}^{-1}$ and on/off ratio of 4.5×10^5 . However, despite its high regularity, PaC4 lacking an aromatic head shows a low μ of $0.35 \text{ cm}^{-2} \text{ V}^{-1} \text{ S}^{-1}$ due to insufficient inductive effect between SAMs and pentacene.^[35,36] V_{th} can be modulated by SAM density and regularity simultaneously. A dense SAM can reduce V_{th} by promoting surface bonding and passivating the surface defects, such as dangling bonds.^[36] On the other hand, high SAM regularity can further improve the effective molecular dipole perpendicular to the substrate (out of plane for p-type semiconductors) to optimize V_{th} on the basis of the inherent dipole of the SAM molecule (Figure S9, Supporting Information).^[34,37]

3. Conclusion

In this work, four SAM molecules with different conjugated groups were designed and utilized to prepare SAMs by kinetic-driven spin-coating. SAMs were carefully evaluated in terms of morphology, density, and regularity. On this basis, a chemical structure-SAM quality model was developed for the SAMs prepared by kinetic-driven spin-coating. As the size of the conjugated group increases, both SAM density and regularity decrease. However, the SAM regularity can be improved when π - π interaction between expanded conjugated groups is strengthened sufficiently. Furthermore, SAMs were applied as the surface modification layer on OFET dielectrics to investigate the influence of SAM quality on OFET properties by key parameters of on/off ratio, μ , and V_{th} . Regular SAMs with conjugated head groups could improve the on/off ratio and μ effectively. On the other hand, V_{th} could be modulated through both SAM density and effective molecular dipoles normal to the substrate. Thus, a three-component relationship was established for chemical structure, SAM quality, and device performance. This work provides an experimental guideline for developing new SAMs, controlling SAM processing, and optimizing SAM-based functional devices.

Supporting Information

Supporting Information is available from the Wiley Online Library or from the author.

Acknowledgements

This work was supported in part by the Hong Kong Research Grants Council (RGC), the Collaborative Research Fund (C7018-20G, C7082-21G), RGC Research Fellowship (RFS2122-7S06), Croucher Foundation Senior Research Fellowship (2022), the Seed Funding for Strategic Interdisciplinary

Research of the University of Hong Kong, and the Hong Kong Quantum AI Lab, AIR@InnoHK of the Hong Kong Government. Computations were done using the National Supercomputing Center in Shenzhen, P. R.China.

Conflict of Interest

The authors declare no conflict of interest.

Author Contributions

J.T. and M.L. conceived and designed the experiments. M.L. performed material synthesis, device fabrication, and most of the device characterizations. Y.C. fabricated the ALD films. K.X. did the theoretical calculation. M.L. and J.T. analyzed the data and wrote the paper. All the authors discussed the results and commented on the manuscript. All authors have given approval to the final version of the manuscript.

Data Availability Statement

The data that support the findings of this study are available in the supplementary material of this article.

Keywords

head engineering, organic field-effect transistor, packing model, self-assembled monolayers, spin-coating

Received: October 18, 2023

Revised: November 5, 2023

Published online:

- [1] A. Ulman, *Chem. Rev.* **1996**, 96, 1533.
- [2] M. Li, Y. Xie, F. R. Lin, Z. Li, S. Yang, A. K.-Y. Jen, *The Innovation* **2023**, 4, 100369.
- [3] S. Casalini, C. A. Bortolotti, F. Leonardi, F. Biscarini, *Chem. Soc. Rev.* **2017**, 46, 40.
- [4] H. Ma, H.-L. Yip, F. Huang, A. K.-Y. Jen, *Adv. Funct. Mater.* **2010**, 20, 1371.
- [5] H. Chen, X. Guo, *Small* **2013**, 9, 1144.
- [6] H. Chen, W. Zhang, M. Li, G. He, X. Guo, *Chem. Rev.* **2020**, 120, 2879.
- [7] F. H. Isikgor, S. Zhumagali, L. V. T. Merino, M. De Bastiani, I. McCulloch, S. De Wolf, *Nat. Rev. Mater.* **2023**, 8, 89.
- [8] Peng Xiao, Linfeng Lan, Ting Dong, Zhenguang Lin, Sheng Sun, Wei Song, Junbiao Peng, *IEEE Electron Device Lett.* **2015**, 36, 687.
- [9] P. Xiao, L. Lan, T. Dong, Z. Lin, W. Shi, R. Yao, X. Zhu, J. Peng, *Appl. Phys. Lett.* **2014**, 104, 051607.
- [10] Y. Lin, Y. Firdaus, F. H. Isikgor, M. I. Nugraha, E. Yengel, G. T. Harrison, R. Hallani, A. El-Labban, H. Faber, C. Ma, X. Zheng, A. Subbiah, C. T. Howells, O. M. Bakr, I. McCulloch, S. D. Wolf, L. Tsetseris, T. D. Anthopoulos, *ACS Energy Lett.* **2020**, 5, 2935.
- [11] H. Bin, K. Datta, J. Wang, T. P. A. Van Der Pol, J. Li, M. M. Wienk, R. A. J. Janssen, *ACS Appl. Mater. Interfaces* **2022**, 14, 16497.
- [12] S. Y. Kim, S. J. Cho, S. E. Byeon, X. He, H. J. Yoon, *Adv. Energy Mater.* **2020**, 10, 2002606.
- [13] F. Li, A. K.-Y. Jen, *Acc. Mater. Res.* **2022**, 3, 272.
- [14] M. Halik, A. Hirsch, *Adv. Mater.* **2011**, 23, 2689.
- [15] S. Whitelam, R. L. Jack, *Annu. Rev. Phys. Chem.* **2015**, 66, 143.
- [16] D. K. Schwartz, *Annu. Rev. Phys. Chem.* **2001**, 52, 107.

- [17] H.-Y. Nie, M. J. Walzak, N. S. McIntyre, *J. Phys. Chem. B* **2006**, *110*, 21101.
- [18] D. Liu, Z. He, Y. Su, Y. Diao, S. C. B. Mannsfeld, Z. Bao, J. Xu, Q. Miao, *Adv. Mater.* **2014**, *26*, 7190.
- [19] D. Yan, J. A. Saunders, G. K. Jennings, *Langmuir* **2000**, *16*, 7562.
- [20] M. Byloos, H. Al-Maznai, M. Morin, *J. Phys. Chem. B* **1999**, *103*, 6554.
- [21] A. Asyuda, M. Gärtner, X. Wan, I. Burkhart, T. Saßmannshausen, A. Terfort, M. Zharnikov, *J. Phys. Chem. C* **2020**, *124*, 8775.
- [22] D. O. Hutchins, T. Weidner, J. Baio, B. Polishak, O. Acton, N. Cernetic, H. Ma, A. K.-Y. Jen, *J. Mater. Chem. C* **2013**, *1*, 101.
- [23] N. B. Arndt, F. Schlüter, M. Böckmann, T. Adolphs, H. F. Arlinghaus, N. L. Doltsinis, B. J. Ravoo, *Langmuir* **2022**, *38*, 735.
- [24] X. Deng, F. Qi, F. Li, S. Wu, F. R. Lin, Z. Zhang, Z. Guan, Z. Yang, C.-S. Lee, A. K.-Y. Jen, *Angew. Chem., Int. Ed.* **2022**, *61*, e202203088.
- [25] A. Ullah, K. H. Park, H. D. Nguyen, Y. Siddique, S. F. A. Shah, H. Tran, S. Park, S. I. Lee, K.-K. Lee, C.-H. Han, K. Kim, S. Ahn, I. Jeong, Y. S. Park, S. Hong, *Adv. Energy Mater.* **2022**, *12*, 2103175.
- [26] G. Wang, M. Li, Q. Wei, Y. Xiong, J. Li, Z. Li, J. Tang, F. Wei, H. Tu, *ACS Sens.* **2021**, *6*, 1849.
- [27] Y. Lin, Y. Zhang, J. Zhang, M. Marcinkas, T. Malinauskas, A. Magomedov, M. I. Nugraha, D. Kaltsas, D. R. Naphade, G. T. Harrison, A. El-Labban, S. Barlow, S. De Wolf, E. Wang, I. McCulloch, L. Tsetseris, V. Getautis, S. R. Marder, T. D. Anthopoulos, *Adv. Energy Mater.* **2022**, *12*, 2202503.
- [28] T. Laredo, J. Leitch, M. Chen, I. J. Burgess, J. R. Dutcher, J. Lipkowski, *Langmuir* **2007**, *23*, 6205.
- [29] M. Ghosh, D.-S. Yang, *Phys. Chem. Chem. Phys.* **2020**, *22*, 17325.
- [30] B. Zhao, B. Gothe, A. Groh, T. Schmaltz, J. Will, H.-G. Steinrück, T. Unruh, S. Mecking, M. Halik, *ACS Appl. Mater. Interfaces* **2021**, *13*, 32461.
- [31] G. G. Ting, O. Acton, H. Ma, J. W. Ka, A. K.-Y. Jen, *Langmuir* **2009**, *25*, 2140.
- [32] R. G. Snyder, H. L. Strauss, C. A. Elliger, *J. Phys. Chem.* **1982**, *86*, 5145.
- [33] H. Chen, S. Dong, M. Bai, N. Cheng, H. Wang, M. Li, H. Du, S. Hu, Y. Yang, T. Yang, F. Zhang, L. Gu, S. Meng, S. Hou, X. Guo, *Adv. Mater.* **2015**, *27*, 2113.
- [34] M. Salinas, C. M. Jäger, A. Y. Amin, P. O. Dral, T. Meyer-Friedrichsen, A. Hirsch, T. Clark, M. Halik, *J. Am. Chem. Soc.* **2012**, *134*, 12648.
- [35] H. S. Lee, D. H. Kim, J. H. Cho, M. Hwang, Y. Jang, K. Cho, *J. Am. Chem. Soc.* **2008**, *130*, 10556.
- [36] H. Ma, O. Acton, D. O. Hutchins, N. Cernetic, A. K.-Y. Jen, *Phys. Chem. Chem. Phys.* **2012**, *14*, 14110.
- [37] Y. Jang, J. H. Cho, D. H. Kim, Y. D. Park, M. Hwang, K. Cho, *Appl. Phys. Lett.* **2007**, *90*, 132104.